Toroidal Rotation Profile Control for the DIII-D Tokamak

William Wehner, Justin Barton, and Eugenio Schuster

***Abstract*— A model-based control approach for the combined regulation of the plasma toroidal angular rotation profile and stored energy for the DIII-D tokamak is proposed in this work. We consider, a first-principles-driven (FPD), control-oriented model of the toroidal rotation profile evolution which incorporates scenario-specific models of the momentum sources. Available rotation control mechanisms include the non-axisymmetric field coils, which provide rotation damping, and the neutral beam injectors (NBI). The plasma stored energy is regulated by the total injected auxiliary power. Optimal state feedback control with integral action is used to regulate the profile around a target while rejecting disturbances. The controller is designed to be robust against uncertainties in the anomalous momentum diffusivity term.**

I. INTRODUCTION

To initiate a fusion reaction on earth, temperatures on the order of $10^7 - 10^9$ K are required to overcome the Coulomb repulsion between like-charged nuclei. The conventional fusion plasma, i.e. a hot gas of hydrogen ions and electrons, must be confined by magnetic fields because the high temperatures required would otherwise melt the confining structure. The motion of ionized particles are tied to the magnetic field lines by the Lorentz force. Therefore, to contain the plasma, a common solution is to close the magnetic field lines in on themselves, forming a torus. When the magnetic field is configured such that the field lines follow a helical path through the torus, the confinement device is called a tokamak. Following any magnetic field line a number of times around the torus maps out a closed flux tube, a so called magnetic-flux surface (Fig. 1) [1].

In a tokamak, each individual particle has its own velocity. The net sum of velocities of a particle species, hydrogen ions for example, is the fluid velocity of that species. The fluid velocity can be separated into components parallel and perpendicular to the flux surfaces. Fluid velocity perpendicular to a flux surface is called convection, and fluid velocity parallel to the flux surface is called rotation [2]. The toroidal shape of a tokamak produces strong poloidal rotation damping [3]. Thus, we consider the toroidal component, V_ϕ, or the angular frequency $\Omega_\phi = V_\phi/R$, where R is the plasma major radius (Fig. 1).

It is generally accepted that plasma rotation can contribute to both stability and confinement in tokamak plasmas. The confinement in a tokamak is governed by the radial transport of energy from the plasma center to the plasma edge. A large part of this transport is driven by turbulence, which is substantially reduced by rotational shear. Plasma toroidal rotation, or its shear, has also been recognized as a stabilizing mechanism for deleterious magnetohydrodynamic (MHD) instabilities such as the neoclassical tearing mode (NTM) [4] and the resistive wall mode (RWM) [5], [6].

NBI is the dominant source of momentum (and therefore rotation) in present-day tokamaks [7]. NBI consists of injecting beams of highly energetic neutral particles into the plasma, heating the plasma through collisions, and naturally transferring momentum. The NBI system at DIII-D [8] consists of eight beam-lines, each of which can inject a maximum of 2.5 MW of power into the plasma. Four NBI are configured to inject in the co-current direction (in the same direction as the plasma current) aligned with the magnetic axis, two beams are configured to drive co-current with alignment off-axis, and the last two beams are configured to inject counter-current (opposite to the plasma current direction) with on-axis alignment. The configuration of each beam type is shown in Fig. 1.

Ambient or purposely imposed non-axisymmetric magnetic fields break down the perfect toroidal symmetry of the containing magnetic field. The toroidal asymmetry leads to a radial current across the plasma which creates an $E \times B$ force in the toroidal direction by interacting with the poloidal magnetic field [9]. Both resonant and non-resonant magnetic field perturbations can affect plasma rotation. However, in this work, we consider only non-resonant magnetic fields (NRMF) since they dominate the impact on rotation [6]. Recent experiments have observed that static NRMF fields tend to drag the rotation to a negative offset [10].

In addition to the NBI and NRMF torque sources, six radio-frequency (RF) wave generators are available to inject energy into the plasma. The RF waves resonate with the gyro-kinetic orbit of the electrons, heating the plasma by an effect known as electron cyclotron resonant heating (ECRH).

In previous work [11], simultaneous control of the bulk rotation and stored energy was considered. In this work, we extend the modeling and control design to consider the entire rotation profile. We focus on high confinement (H-mode) advanced tokamak (AT) plasma scenarios, those characterized by a transport barrier just inside the plasma boundary [12]. The model structure is described in Section II, details of the model order reduction using the finite element method and the modeling of the uncertain momentum diffusivity are given in Section III, model-based control design for simultaneous regulation of the rotation and stored energy is performed in Section IV, robust stability analysis is carried out in Section V, and, finally, the effectiveness of the controller is examined in Section VI via a simulation study.

This work was supported in part by the U.S. Department of Energy (DE-SC0010661). W. Wehner (`wehner@lehigh.edu`), J. Barton, and E. Schuster are with the Department of Mechanical Engineering and Mechanics, Lehigh University, Bethlehem, PA 18015, USA.

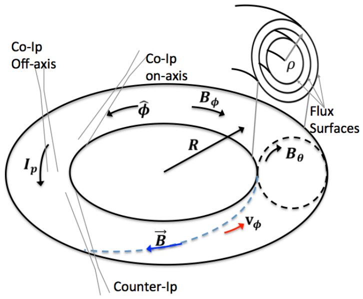

Fig. 1. Tokamak toroidal geometry with toroidal (B_ϕ) and poloidal (B_θ) field components and toroidal ($\hat{\phi}$) and poloidal ($\hat{\theta}$) directions indicated. The plasma current, I_p, is the primary source of the poloidal field. Also shown are the configurations of various neutral beam injectors relative to the plasma current direction. From the indicated direction of V_ϕ, it is apparent that the co-current NBI drive rotation and the counter-current NBI slow rotation.

II. Modeling the Toroidal Angular Rotation

As a spatial coordinate, this work makes use of the mean effective minor radius, ρ. It can be expressed in terms of the toroidal magnetic flux, Φ, and the toroidal field strength at the plasma center, $B_{\phi,0}$, i.e. $\pi B_{\phi,0}\rho^2 = \Phi$. Normalized ρ, denoted by $\hat{\rho}$, is defined as ρ/ρ_b, where ρ_b is the value of ρ at the last closed magnetic flux surface. To model the rotation profile evolution we make the following simplifying assumptions: *i)* the angular momentum associated with the electrons is negligible, *ii)* the plasma shape is fixed, *iii)* the plasma ions can be modeled as a single fluid species, and *iv)* the momentum transport is purely diffusive. With these assumptions the evolution of toroidal angular momentum, $P_\phi = m_\mathrm{i} n_\mathrm{i} \langle R^2 \rangle \Omega_\phi$ reduces to [13]

$$\begin{aligned} n_\mathrm{i} m_\mathrm{i} \langle R^2 \rangle \frac{\partial \Omega_\phi}{\partial t} + m_\mathrm{i} \langle R^2 \rangle \Omega_\phi \frac{\partial n_\mathrm{i}}{\partial t} = \eta_\mathrm{NB} + \eta_\mathrm{NR} \\ + \frac{1}{\hat{\rho}\hat{H}} \frac{\partial}{\partial \hat{\rho}} \left[\hat{\rho} \hat{H} n_\mathrm{i} m_\mathrm{i} \chi_\phi \langle R^2 \left(\nabla \hat{\rho}\right)^2 \rangle \frac{\partial \Omega_\phi}{\partial \hat{\rho}} \right], \end{aligned} \tag{1}$$

where m_i and n_i, are the single fluid ion mass and ion density, χ_ϕ is the effective angular momentum diffusivity coefficient, $\eta_{(\cdot)}$ represents the local torque density from NBI and NRMF sources, the operator $\langle \cdot \rangle$ stands for flux surface average, R is the major radius of the plasma (see Fig. 1), and $\hat{H}$ is a spatial geometric factor specific to the magnetic configuration in the DIII-D tokamak. The boundary conditions are determined from symmetry at the plasma center and an assumed no slip condition[1] at the plasma edge,

$$\partial \Omega_\phi / \partial \hat{\rho}(0,t) = 0, \qquad \Omega_\phi(1,t) = 0. \tag{2}$$

Scenario-specific empirical models of the ion density and temperature profiles, and torque sources are used to obtain a control-oriented model of the toroidal rotation profile evolution.

1) Ion Density Modeling: Assuming rotation control is limited to the H-mode regime, the control action employed to regulate the line-averaged ion density can be fairly approximated as only weakly affecting the radial distribution of the ions. Therefore, the ion density $n_\mathrm{i}(\hat{\rho},t)$ is modeled as

$$n_\mathrm{i}(\hat{\rho},t) = n_\mathrm{i}^\mathrm{prof}(\hat{\rho}) \bar{n}_\mathrm{i}(t), \tag{3}$$

where $n_\mathrm{i}^\mathrm{prof}(\hat{\rho})$ is a reference profile, and $\bar{n}_\mathrm{i}$ is the line averaged density.

2) Ion Temperature Modeling: The slowly evolving ion temperature profile evolution can be modeled according to the scaling law [14]

$$T_\mathrm{i}(\hat{\rho},t) = k_{T_\mathrm{i}}^\mathrm{prof}(\hat{\rho}) \frac{T_\mathrm{i}^\mathrm{prof}(\hat{\rho})}{n_\mathrm{i}^\mathrm{prof}(\hat{\rho})} \frac{I_\mathrm{p}(t)\sqrt{P_\mathrm{tot}(t)}}{\bar{n}_\mathrm{i}(t)} \tag{4}$$

where $T_\mathrm{i}^\mathrm{prof}(\hat{\rho})$ is a reference ion temperature profile, $I_\mathrm{p}(t)$ is the total plasma current, $P_\mathrm{tot}(t)$ is the total power absorbed by the plasma, and $k_{T_\mathrm{i}}^\mathrm{prof}(\hat{\rho})$ is a constant scaling profile. The total absorbed power is equal to the auxiliary power injected into the plasma by NBI and ECRH, $P_\mathrm{aux} = \sum_\xi^{n_\mathrm{NB}} P_{\mathrm{NB},\xi} + P_\mathrm{EC}$, plus the power from the ohmic coil, P_ohm, minus the radiative power, P_rad. The ohmic and radiative powers are functions of the poloidal flux and electron temperature and density for which mature control-oriented models have been developed [15].

3) NBI Torque: For the torque density deposited by each neutral beam line we propose the scaling law,

$$\begin{aligned} \eta_{\mathrm{NB},\xi}(\hat{\rho},t) = k_{\mathrm{NB},\xi}^\mathrm{prof}(\hat{\rho}) \eta_{\mathrm{NB},\xi}^\mathrm{prof}(\hat{\rho}) \\ \times\ n_\mathrm{i}(\hat{\rho},t)^{\gamma_n} T_\mathrm{i}(\hat{\rho},t)^{\gamma_T} P_{\mathrm{NB},\xi}(t), \end{aligned} \tag{5}$$

where $P_{\mathrm{NB},\xi}(t)$ is the power for each neutral beam line, $\eta_{\mathrm{NB},\xi}^\mathrm{prof}(\hat{\rho})$ is the torque density reference profile for each beam, and $k_{\mathrm{NB},\xi}^\mathrm{prof}(\hat{\rho})$ is a constant scaling profile. The scalings $\gamma_n = -1.1$ and $\gamma_T = 0.1$ are determined by a linear regression fit to data based on DIII-D shot 147634. The individual beam lines are labeled according to their orientation with the plasma (30L, 30R, 150L, 150R, 210L, 210R, 330L, 330R). Of these, 30L and 30R are used for diagnostics and, therefore, not considered available for rotation control. Throughout the paper, the label $\xi = 1, \ldots, n_\mathrm{NB}$ is used to index the beam lines: $\xi = 1$ refers to 30L, $\xi = 2$ refers to 30R, etc.

4) NRMF Torque: The NRMF torque density is dependent on the collisionality regime of the plasma [16], thus dependent on temperature and density,

$$\begin{aligned} \eta_\mathrm{NR}(\hat{\rho},t) = k_\mathrm{NR}^\mathrm{prof}(\hat{\rho}) \eta_\mathrm{NR}^\mathrm{prof}(\hat{\rho}) \left(\Omega_\phi(\hat{\rho},t) - \Omega_\phi^*(\hat{\rho}) \right) \\ \times\ n_\mathrm{i}(\hat{\rho},t)^{\alpha_n} T_\mathrm{i}(\hat{\rho},t)^{\alpha_T} \omega_E(\hat{\rho})^{\alpha_\omega} I_\mathrm{NRMF}(t)^2, \end{aligned} \tag{6}$$

where $I_\mathrm{NRMF}(t)$ is the current in the perturbation field coils, $\Omega_\phi^*(\hat{\rho})$ is an offset rotation, $\omega_E(\hat{\rho})$ is the toroidal component of the $E \times B$ drift velocity, $\eta_\mathrm{NR}^\mathrm{prof}(\hat{\rho})$ is a reference profile, $k_\mathrm{NR}^\mathrm{prof}(\hat{\rho})$ is a constant scaling profile, and the scalings are $\alpha_n = 3.6$, $\alpha_T = 2.6$, and $\alpha_\omega = -0.6$ [17].

The parameters $\langle R^2 \rangle(\hat{\rho})$, $\langle R^2 (\nabla \hat{\rho})^2 \rangle(\hat{\rho})$, and $\hat{H}(\hat{\rho})$ do not change significantly during the plasma current flattop phase of a discharge, thus we elect to approximate them as fixed spatial profiles. The profiles are obtained from a TRANSP simulation of DIII-D shot 147634. Modeling of the effective diffusivity term, χ_ϕ, which is partly composed of turbulent

[1]The rotation at the edge is negligible compared to the bulk rotation for typical H-mode, NBI heated plasmas.

effects, is not considered in this work. Instead, we select a constant nominal profile shape based on the time average of the measured diffusivity from DIII-D shot 147634 as shown in Fig. 2(c). In the control development sections that follow, variations of χ_ϕ from the nominal profile will be modeled as an uncertainty.

5) Plasma Stored Energy: The volume averaged plasma stored energy balance is given by

$$dE/dt = -E/\tau_{\mathrm{E}} + P_{\mathrm{tot}}(t), \tag{7}$$

where τ_{E} is a the global energy confinement time. The IPB98$(y, 2)$ scaling law ([18]) has been adopted to model energy confinement time scaling.

III. Model Order Reduction

A. Toroidal Rotation Evolution: Control Form

To simplify the control development, the rotation evolution model (1) is combined with the scenario specific models for density (3), temperature (4), and momentum sources (5)-(6) and rewritten in the form

$$\begin{aligned}\frac{\partial \Omega_\phi}{\partial t} &= \frac{1}{\hat{\rho}} f_1 \frac{\partial}{\partial \hat{\rho}}\left(\hat{\rho} f_2 \chi_\phi \frac{\partial \Omega_\phi}{\partial \hat{\rho}}\right) + \sum_{\xi=1}^{n_{\mathrm{NB}}} f_{\mathrm{NB},\xi} u_{\mathrm{NB},\xi} \\ &+ (\Omega_\phi - \Omega_\phi^\star) f_{\mathrm{NR}} u_{\mathrm{NR}} - \Omega_\phi u_{\bar{n}_{\mathrm{i}}},\end{aligned} \tag{8}$$

where the functions $f_{(\cdot)}(\hat{\rho})$ incorporate constant profile shapes and $u_{(\cdot)}(t)$ are a set of nonlinear input functions,

$$\begin{aligned} u_{\bar{n}_{\mathrm{i}}} &= \frac{\dot{\bar{n}}_{\mathrm{i}}}{\bar{n}_{\mathrm{i}}}, \quad u_{\mathrm{NB},\xi} = \left(\frac{I_{\mathrm{p}}\sqrt{P_{\mathrm{tot}}}}{\bar{n}_{\mathrm{i}}}\right)^{\gamma_T} \bar{n}_{\mathrm{i}}^{\gamma_n} \frac{P_{\mathrm{NB},\xi}}{\bar{n}_{\mathrm{i}}}, \\ u_{\mathrm{NR}} &= \left(\frac{I_{\mathrm{p}}\sqrt{P_{\mathrm{tot}}}}{\bar{n}_{\mathrm{i}}}\right)^{\alpha_T} \bar{n}_{\mathrm{i}}^{\alpha_n} \frac{I_{\mathrm{NRMF}}^2}{\bar{n}_{\mathrm{i}}}.\end{aligned} \tag{9}$$

B. Discretization by Finite Element Method

The infinite-dimensional model (8) in $\hat{\rho}$ is transformed into a finite-dimensional model using the finite-element method. First, the rotation and diffusivity term are approximated by

$$\Omega_\phi(\hat{\rho}, t) \approx \sum_{k=1}^{l_\omega} \omega_k(t) \phi_k(\hat{\rho}), \quad \chi_\phi(\hat{\rho}, t) \approx \sum_{\alpha=1}^{l_\chi} \gamma_\alpha \varphi_\alpha(\hat{\rho}), \tag{10}$$

where the basis $\{\phi_k \mid k = 1, 2, \ldots, l_\omega\}$, is chosen as a set of cubic splines (Fig. 2(a)) on a finite support that satisfy the boundary conditions (2). The basis $\{\varphi_\alpha \mid \alpha = 1, 2, \ldots, l_\chi\}$ is obtained by the proper orthogonal decomposition (POD) method [19]. The basis obtained for χ_ϕ based on DIII-D shot 147634 is shown in Fig. 2(b), as well as the expected range modeled as a linear combination of the modes in Fig. 2(c). The POD method has the capability of obtaining a basis with relatively lower dimension than a spline basis.

Substituting (10) into the evolution for Ω_ϕ (8), we have

$$\begin{aligned}\sum_{k=1}^{l_\omega} \frac{\mathrm{d}\omega_k}{\mathrm{d}t} \phi_k &= \sum_{k=1}^{l_\omega} \sum_{\alpha=1}^{l_\chi} \omega_k \gamma_\alpha \frac{f_1}{\hat{\rho}} \frac{\partial}{\partial \hat{\rho}}\left[\hat{\rho} f_2 \varphi_\alpha \frac{\partial \phi_k}{\partial \hat{\rho}}\right] - \omega_k \phi_k u_{\bar{n}_{\mathrm{i}}} \\ &+ \sum_{\xi=1}^{n_{\mathrm{NB}}} f_{\mathrm{NB},\xi} u_{\mathrm{NB},\xi} + \left(\sum_{k=1}^{l_\omega} \omega_k \phi_k - \Omega_\phi^\star\right) f_{\mathrm{NR}} u_{\mathrm{NR}}.\end{aligned} \tag{11}$$

where dependencies on $\hat{\rho}$ and t have been dropped for notational convenience. Next, we construct the *weak form* by multiplying both sides with $\hat{\rho}$, projecting onto the trial functions ϕ_j, $j = 1, \ldots, l_\omega$ and integrating over the domain, to obtain

$$\begin{aligned}\sum_{k=1}^{l_\omega} \frac{\mathrm{d}\omega_k}{\mathrm{d}t} M_{jk} &= -\sum_{k=1}^{l_\omega} \omega_k M_{jk} u_{\bar{n}_{\mathrm{i}}} + \omega_k S_{jk} \\ &+ \sum_{\xi=1}^{n_{\mathrm{NB}}} B_{\mathrm{NB},j\xi} u_{\mathrm{NB},\xi} + \sum_{k=1}^{l_\omega} \omega_k B_{\mathrm{NR},jk} u_{\mathrm{NR}} - B_{\mathrm{NR},j}^\star u_{\mathrm{NR}},\end{aligned} \tag{12}$$

where $F' = \frac{\partial F}{\partial \hat{\rho}}$. Introducing the notation $\langle\langle g_1, \ldots, g_N \rangle\rangle \triangleq \int_0^1 g_1(\hat{\rho}) \ldots g_N(\hat{\rho}) \hat{\rho} d\hat{\rho}$, we have

$$\begin{aligned} M_{jk} &= \langle\langle \phi_j, \phi_k \rangle\rangle, \quad B_{\mathrm{NB},j\xi} = \langle\langle \phi_j, f_{\mathrm{NB},\xi} \rangle\rangle, \\ S_{jk} &= \sum_{\alpha=1}^{l_\chi} \gamma_\alpha \left(\langle\langle f_1 \phi_j', \phi_k', f_2 \varphi_\alpha \rangle\rangle + \langle\langle f_1' \phi_j, \phi_k', f_2 \varphi_\alpha \rangle\rangle\right), \\ B_{\mathrm{NR},jk} &= \langle\langle \phi_j, \phi_k, f_{\mathrm{NR}} \rangle\rangle, \quad B_{\mathrm{NR},j}^\star = \langle\langle \phi_j, \Omega_\phi^\star, f_{\mathrm{NR}} \rangle\rangle,\end{aligned} \tag{13}$$

which allows the system to be written in the matrix form

$$\begin{aligned} M \frac{d\omega}{dt} &= -M\omega u_{\bar{n}_{\mathrm{i}}} - S\omega + \sum_{\xi=1}^{n_{\mathrm{NB}}} B_{\mathrm{NB},\xi} u_{\mathrm{NB},\xi}(t) \\ &+ B_{\mathrm{NR}} \omega u_{\mathrm{NR}} - B_{\mathrm{NR}}^\star u_{\mathrm{NR}}.\end{aligned} \tag{14}$$

C. Uncertainty Modeling for Momentum Diffusivity (χ_ϕ)

Since the effective diffusivity, χ_ϕ, is assumed to include contributions of turbulent effects which are not sufficiently understood to obtain a reliable model, we chose to represent it as an uncertainty. The parameter $\gamma = (\gamma_1, ..., \gamma_{l_\chi}) \in \mathbb{R}^{l_\chi}$ of (10) is the uncertainty vector representing a finite dimensional approximation of $\chi_\phi(\hat{\rho}, t)$ with respect to the basis $\{\varphi_\alpha \mid \alpha = 1, \ldots, l_\chi\}$. Each γ_α has the form $\gamma_\alpha = \gamma_\alpha^0 + \gamma_\alpha^1 \delta_\alpha$, where γ_α^0 and γ_α^1 are constants and $|\delta_\alpha| \leq 1$ for all α.

To make the uncertainty in the state-space system explicit, the matrix S (13) can be decomposed as

$$\begin{aligned} S &= \hat{S}^0 + \sum_{\alpha=1}^{l_\chi} \delta_\alpha \hat{S}^\alpha, \\ \hat{S}_{jk}^0 &= \sum_{\alpha=1}^{l_\chi} \gamma_\alpha^0 \left(\langle\langle f_1 \phi_j', \phi_k', f_2 \varphi_\alpha \rangle\rangle + \langle\langle f_1' \phi_j, \phi_k', f_2 \varphi_\alpha \rangle\rangle\right), \\ \hat{S}_{jk}^\alpha &= \gamma_\alpha^1 \left(\langle\langle f_1 \phi_j', \phi_k', f_2 \varphi_\alpha \rangle\rangle + \langle\langle f_1' \phi_j, \phi_k', f_2 \varphi_\alpha \rangle\rangle\right).\end{aligned} \tag{15}$$

Combining (14) and (15), we obtain a nonlinear, finite dimensional, ordinary differential equation model defined by

$$\dot{\omega} = F(\omega, u, \delta) \tag{16}$$

where $\omega = (\omega_1, \ldots, \omega_{l_\omega}) \in \mathbb{R}^{l_\omega}$, $\delta = (\delta_1, \ldots, \delta_{l_\chi}) \in \mathbb{R}^{l_\chi}$, and $u = (\dot{\bar{n}}_{\mathrm{i}}, \bar{n}_{\mathrm{i}}, P_{\mathrm{EC}}, P_{\mathrm{NB},1}, \ldots, P_{\mathrm{NB},n_{\mathrm{NB}}}, I_{\mathrm{NRMF}}) \in \mathbb{R}^{4+n_{\mathrm{NB}}}$.

IV. Control System Design

In this section, a multi-input-multi-output (MIMO) feedback controller based on the FPD model (1)-(2) is proposed for the simultaneous regulation of the toroidal angular rotation profile and stored energy for DIII-D.

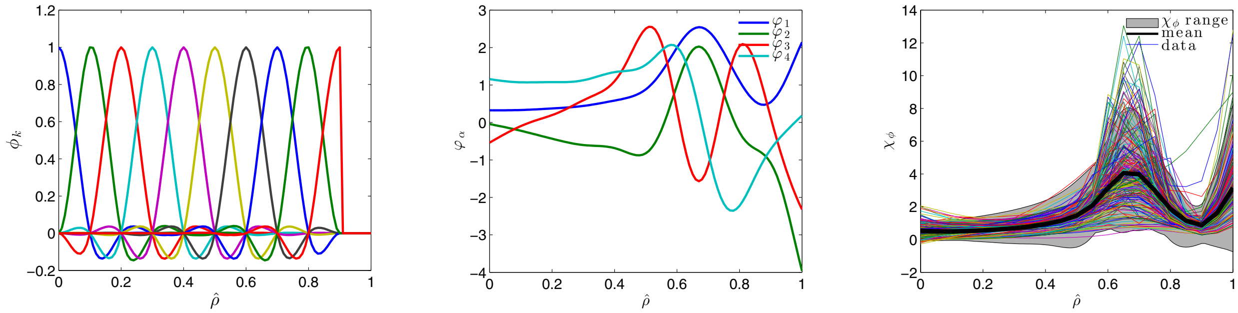

(a) Cubic splines (b) POD modes (c) χ_ϕ

Fig. 2. (a.) Cubic splines which serve as a basis for Ω_ϕ. (b.) POD modes which serve as a basis for χ_ϕ. (c.) The time average of χ_ϕ (black line) based on DIII-D shot 147634 over the time period $t = 2 - 5$ s, i.e. the current flattop phase and the expected range of χ_ϕ (grey area).

A. Model Linearization

The plasma density in tokamaks is extremely difficult to control with any real precision, therefore deviations of the density from the desired operating point will be treated as an input disturbance. To account for this we split the input u into the controlled input $u_1 = (P_{\text{EC}}, P_{\text{NB},3}, \ldots, P_{\text{NB},n_{\text{NB}}}, I_{\text{NRMF}})$ and the uncontrolled input $u_2 = (P_{\text{NB},1}, P_{\text{NB},2}, \dot{\bar{n}}_{\text{i}}, \bar{n}_{\text{i}})$. Linearizing the system (16) with respect to the state and control input around a nominal equilibrium point $(\omega_{\text{eq}}, u_{\text{eq}})$, we obtain the linear time-invariant model given by

$$\dot{x}_\omega = A_\omega x_\omega + B_\omega u_{\text{FB}} + B_{\omega,\text{d}} u_{\text{d}}, \tag{17}$$

where $x_\omega = \omega - \omega_{\text{eq}}$, $u_{\text{FB}}(t) = u_1(t) - u_{1,\text{eq}}$, $u_{\text{d}}(t) = u_2(t) - u_{2,\text{eq}}(t)$, $A_\omega = \nabla_\omega F|_{\omega_{eq}, u_{eq}}$, $B_\omega = \nabla_v F \nabla_{u_1} v|_{\omega_{eq}, u_{eq}}$, and $B_{\omega,\text{d}} = \nabla_v F \nabla_{u_2} v|_{\omega_{eq}, u_{eq}}$, where v represents the nonlinear input functions, $v = (u_{\bar{n}_{\text{i}}}, u_{\text{NB},1}, \ldots, u_{\text{NB},n_{\text{NB}}}, u_{\text{NR}})$. For control design we consider the nominal system, i.e. $\delta = 0$.

The stored energy evolution (7) is approximated by $dE/dt = -E/\tau_{\text{E}_{\text{eq}}} + P_{\text{aux}}(t)$, where the contributions of ohmic power and radiative power are dropped since they are relatively small compared to the auxiliary power for H-mode plasmas, and $\tau_{\text{E}_{\text{eq}}}$ is the global energy confinement time associated with the equilibrium point $(\omega_{\text{eq}}, u_{\text{eq}})$. An augmented state-space system, $x = (E, x_\omega) \in \mathbb{R}^{1+l_\omega}$, is obtained by lumping the energy evolution together with the linearized rotation evolution,

$$\frac{\mathrm{d}}{\mathrm{dt}} \begin{bmatrix} E \\ x_\omega \end{bmatrix} = \underbrace{\begin{bmatrix} -1/\tau_{\text{E}_{\text{eq}}} & 0 \\ 0 & A_\omega \end{bmatrix}}_{A} \begin{bmatrix} E \\ x_\omega \end{bmatrix} + \underbrace{\begin{bmatrix} (\mathbf{1}, 0)^T \\ B_\omega \end{bmatrix}}_{B} u_{\text{FB}}, \tag{18}$$

where $\mathbf{1}$ is a column of $1 + n_{\text{NB}}$ ones.

B. Singular Value Decomposition

For a requested target state, x_{t}, let x_∞^{ss} represent the closest stationary state achievable according to the model. This can be determined from the pseudo-inverse, $K_{\text{sg}}^\dagger$, of the model static gain matrix $K_{\text{sg}} = -A^{-1}B$. The input associated with the desired target is determined from the pseudo-inverse of the static gain matrix, $u_{\text{FB},\infty}^{ss} = K_{\text{sg}}^\dagger x_{\text{t}}$, which is used to determine the closest achievable stationary state given by $x_\infty^{ss} = K_{\text{sg}} u_{\text{FB},\infty}^{ss} = K_{\text{sg}} K_{\text{sg}}^\dagger x_{\text{t}}$. Because several of the actuators have similar effects on the profile, the matrix $K_{\text{sg}} = W \Sigma V^T$ is ill-conditioned, i.e. the ratio of the largest singular value to the smallest one is much larger than one. Therefore small deviations in the profile associated with the directions of the smaller singular values can result in unreasonably large control requests. Thus, we use a truncated (Tr) singular value expansion of the static gain matrix given by, $K_{\text{sg,Tr}} = W_{\text{Tr}} \Sigma_{\text{Tr}} V_{\text{Tr}}^T$, where the matrices W_{Tr}, Σ_{Tr}, and V_{Tr} are the components of the SVD associated with the n_{SV} largest singular values,

$$W = \begin{bmatrix} W_{\text{Tr}} & W_{\text{n}} \end{bmatrix}, \ \Sigma = \begin{bmatrix} \Sigma_{\text{Tr}} & 0 \\ 0 & \Sigma_{\text{n}} \end{bmatrix}, \ V = \begin{bmatrix} V_{\text{Tr}} & V_{\text{n}} \end{bmatrix}, \tag{19}$$

and W_n, Σ_n, and V_n are the components associated with the smaller, neglected singular values. Therefore,

$$u_{\text{FB},\infty}^{ss} \cong u_{\text{FB},\infty} = K_{\text{sg,Tr}}^\dagger x_t, \ \ x_\infty^{ss} \cong x_\infty = K_{\text{sg,Tr}} K_{\text{sg,Tr}}^\dagger x_t. \tag{20}$$

We use the theory of linear quadratic optimal control to obtain a control law which regulates the system to the closest achievable stationary state while minimizing the cost function

$$J = \int_0^\infty \left[\tilde{x}^T(t) \ \zeta^T(t) \right] Q \begin{bmatrix} \tilde{x}(t) \\ \zeta(t) \end{bmatrix} + \tilde{u}^T(t) R \tilde{u}(t) dt, \tag{21}$$

where $\tilde{x} = x - x_\infty$, $\tilde{u} = u_{\text{FB}} - u_{\text{FB},\infty}$, Q positive semidefinite, R positive definite, and ζ represents the integral states introduced for integral control. The added integral states are expressed as $\zeta = K_\zeta \int_0^t \tilde{x}(\tau) d\tau$, where K_ζ is a design matrix.

C. Choice of Matrix K_ζ

With the choice $K_\zeta = W_{\text{Tr}}^T$, we have $K_\zeta K_{\text{sg,Tr}} K_{\text{sg,Tr}}^\dagger = K_\zeta$, since

$$\left[W_{\text{Tr}}^T \right] \cdot \left[W_{\text{Tr}} \Sigma_{\text{Tr}} V_{\text{Tr}}^T \right] \cdot \left[V_{\text{Tr}} \Sigma_{\text{Tr}}^{-1} W_{\text{Tr}}^T \right] = W_{\text{Tr}}^T = K_\zeta, \tag{22}$$

which ensures $K_\zeta x_{\text{t}} \to K_\zeta x_\infty$, since $x_\infty = K_{\text{sg,Tr}} u_{\text{FB},\infty} = K_{\text{sg,Tr}} K_{\text{sg,Tr}}^\dagger x_{\text{t}}$. Here, we have made use of the fact that $W_{\text{Tr}}^T W_{\text{Tr}} = I$, and $V_{\text{Tr}}^T V_{\text{Tr}} = I$, but $W_{\text{Tr}} W_{\text{Tr}}^T \neq I$.

D. Proportional plus integral control

Written in terms of the requested target ($\tilde{x}(t) = x(t) - K_{\text{sg,Tr}} K_{\text{sg,Tr}}^\dagger x_t(t)$), the control law that minimizes (21) reduces to a proportional plus integral controller of the form

$$\begin{aligned} \tilde{u}(t) = & -K_{\text{p}} \left[x(t) - K_{\text{sg,Tr}} K_{\text{sg,Tr}}^\dagger x_t(t) \right] \\ & - K_{\text{i}} K_\zeta \int_0^t \mathrm{d}\tau \left[x(\tau) - K_{\text{sg,Tr}} K_{\text{sg,Tr}}^\dagger x_t(\tau) \right], \end{aligned} \tag{23}$$

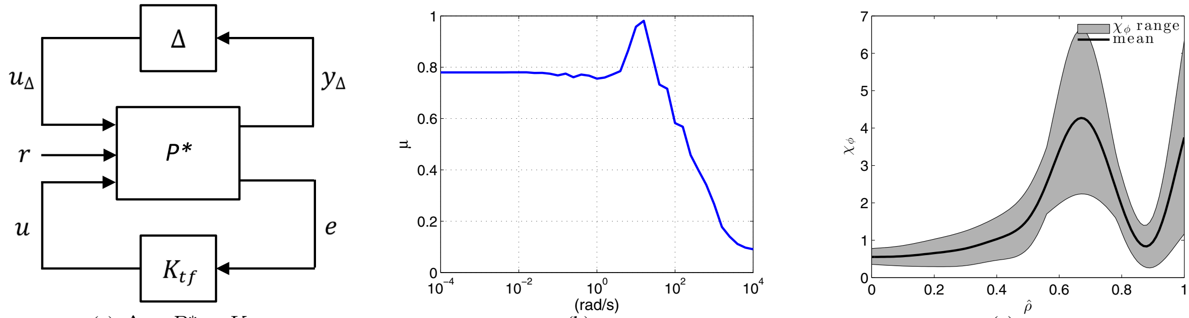

(a) $\Delta - P^* - K_{tf}$ (b) μ (c) χ_ϕ

Fig. 3. (a.) The $\Delta - P^* - K_{tf}$ robust control design framework. (b.) The structured singular value μ. (c.) The Range of χ_ϕ for which robust stability criterion is satisfied.

where the proportional gain, K_p, and integral gain, K_i, are given by $\begin{bmatrix} K_\mathrm{p} & K_\mathrm{i} \end{bmatrix} = R^{-1}\hat{B}S$, where $S = S^T$ is the unique positive semi-definite solution to the algebraic Ricatti equation, $\hat{A}^T S + S\hat{A} - S\hat{B}R^{-1}\hat{B}^T S + Q = 0$, and the system $(\hat{A}, \hat{B})$ is constructed by augmenting the model (17) with the integrator states, i.e.

$$\begin{bmatrix} \dot{\tilde{x}} \\ \dot{\zeta} \end{bmatrix} = \underbrace{\begin{bmatrix} A & 0 \\ K_\zeta & 0 \end{bmatrix}}_{\hat{A}} \begin{bmatrix} \tilde{x} \\ \zeta \end{bmatrix} + \underbrace{\begin{bmatrix} B \\ 0 \end{bmatrix}}_{\hat{B}} \tilde{u}. \tag{24}$$

The design parameters include $K_\zeta = W_{\mathrm{Tr}}^T$, Q and R. The state weighting matrix, Q, is chosen as $Q = \begin{bmatrix} \hat{Q} & 0 \\ 0 & \alpha_\zeta^2 I_{n_\mathrm{sv}} \end{bmatrix}$, where α_ζ is a constant that weights the integrator states relative to the model states, $\hat{Q}$ is the weighting on the model states and R is chosen diagonal.

V. Model in Robust Control Framework

The transfer function of a linear state-space system with representation A, B, C, D can be written as an upper linear fractional transformation (LFT), $G(s) = F_U(M_a, 1/sI) = D + C(sI - A^{-1})B$, where F_U denotes the upper LFT, s is complex variable, and the matrix M_a is defined as

$$M_a = \begin{bmatrix} A & B \\ C & D \end{bmatrix}. \tag{25}$$

For robustness analysis, the linearized state space system (17) can be written as the general linear state-space uncertainty

$$M_a = \begin{bmatrix} A_0 + \sum_{\alpha=1}^{l_\chi} \delta_\alpha A_\alpha & B_0 + \sum_{\alpha=1}^{l_\chi} \delta_\alpha B_\alpha \\ C_0 + \sum_{\alpha=1}^{l_\chi} \delta_\alpha C_\alpha & D_0 + \sum_{\alpha=1}^{l_\chi} \delta_\alpha D_\alpha \end{bmatrix}, \tag{26}$$

where

$$A_0 = \mathrm{diag}\left\{ -\frac{1}{\tau_{E_\mathrm{eq}}}, -u_{\bar{n}_\mathrm{i}} - M^{-1}(\hat{S}^0 + B_\mathrm{NR}u_\mathrm{NR})\Big|_{\omega_{eq}, u_{eq}} \right\},$$

$A_\alpha = \mathrm{diag}\{0, -M^{-1}\hat{S}^\alpha\}$, $B_0 = B$, $B_\alpha = 0$, $C_0 = I$, $C_\alpha = 0$, $D_0 = 0$, and $D_\alpha = 0$.

Let K_{tf} represent the transfer function of the controller obtained in Section IV-D and let $\Delta = \mathrm{diag}\{\delta\}$, then we can form the standard $\Delta - P - K_{tf}$ configuration (Fig. 3(a)) by employing the method outlined in [20], which exploits the structure of the state matrices in (26). See [21] for an example of this technique. If the generalized plant is partitioned as

$$P^\star = \begin{bmatrix} \bar{P}_{11}^\star & \bar{P}_{12}^\star \\ \bar{P}_{21}^\star & \bar{P}_{22}^\star \end{bmatrix}, \qquad \begin{aligned} y_\Delta &= \bar{P}_{11}^\star u_\Delta + \bar{P}_{12}^\star u, \\ e &= \bar{P}_{21}^\star u_\Delta + \bar{P}_{22}^\star u, \end{aligned} \tag{27}$$

the system can be written in the $N - \Delta$ form by using the definition of lower LFT between $P^\star$ and K_{tf},

$$N = F_L(P^\star, K_{tf}) = \bar{P}_{11}^\star + \bar{P}_{12}^\star K_{tf}(I - \bar{P}_{22}^\star K_{tf})^{-1}\bar{P}_{21}^\star. \tag{28}$$

We can compute the structured singular value $\mu(N_{11}(j\omega))$ to determine the robust stability of the closed-loop system, where N_{11} is the transfer function between y_Δ and u_Δ. The closed-loop system is robustly stable for all allowable perturbations if and only if $\mu(N_{11}(j\omega)) < 1$, $\forall\omega$ [22]. To analyze the robust stability of the closed-loop system, a plot of μ versus frequency is shown in Fig. 3(b). To obtain this μ value, the value of χ_ϕ is allowed to vary throughout the range shown in Fig. 3(c) with profile shapes equal to a linear combination of the POD modes in Fig. 2(c).

VI. Simulation Results

In this section, we present a simulation study of the controller's effectiveness. The target for Ω_ϕ is obtained from (1) with the input values and parameter profiles of DIII-D shot 147634, and the stored energy target is simply set to 1 MW, a typical value for H-mode plasmas. Constant feedforward values are used for the NBI, and the feedforward value of the NRMF coil current is set to a ramping function. The selected feedforward input values constitute a large input disturbance from the input values of DIII-D shot 147634 used to determine the target profile shape.

The tuning problem consists of the selection of the diagonal elements of Q and R and the constant α_ζ to regulate the profile as close as possible to the target while maintaining constant stored energy.

In Fig. 4, we test the controller's tracking performance with feedback ON throughout the simulation. The target profile and simulated closed-loop profile response are plotted in 4(a), and the feedforward and requested actuator powers are plotted in Fig. 4(b). The controller performs well, enabling tight profile regulation while maintaining a nearly flat stored energy. At $t = 4$ s, the rotation profile target switches discretely to a lower target value. Note, the controller obtains the second, lower rotation target by increasing the counter

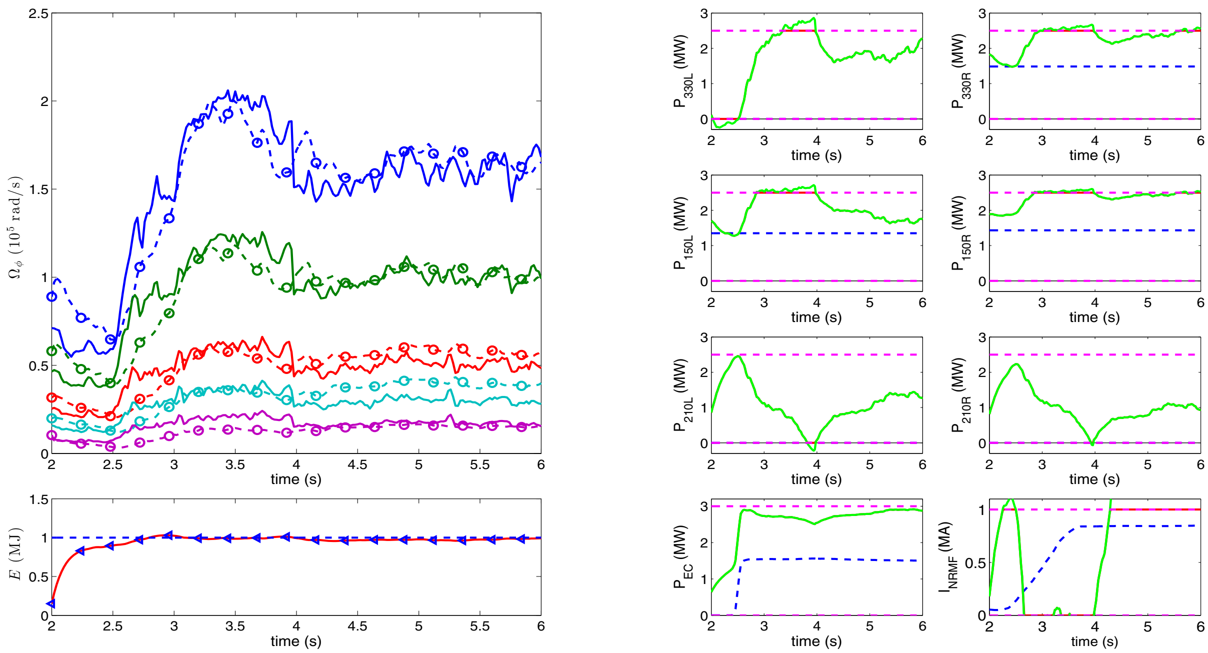

(a) Ω_ϕ and E (b) Inputs

Fig. 4. Feedback control simulation. (a.) Ω_ϕ and E, where the solid line is the target and the achieved profile is marked by circles. The stored energy set point is marked by the blue dashed line. (b.) Input values, where the green line marks the controller requested power, the blue dashed line marks the feedforward power, and the pink dashed line marks the actuators limits.

NBI power (P_{210L} and P_{210R}) while reducing the co NBI power (P_{330L} and P_{150L}) to maintain the stored energy around the set point of 1 MW. The additional power from the ECRH is quite advantageous in maintaining the stored energy value and the NRMF provides some advantage over NBI in regulating the rotation at the plasma edge.

VII. Summary and Conclusions

A robust feedback control algorithm for the simultaneous regulation of toroidal angular rotation and stored energy in advanced plasma scenarios was designed by employing a physics-based model of the plasma dynamics. Using the theory of linear-quadratic optimal control, we synthesized a controller to minimize the weighted tracking error of the rotation profile while maintaining constant stored energy. The simulations show promise of an effective controller for the combined control of rotation and energy using NBI, ECRH, and NRMF coils as actuators.

References

[1] A. Pironti and M. Walker, "Fusion, tokamaks, and plasma control: an introduction and tutorial," *IEEE, Control Systems*, vol. 25, no. 5, pp. 30–43, 2005.

[2] M. D. Bock, "Understanding and controlling plasma rotation in tokamaks," Ph.D. dissertation, Technische Universiteit Eindhoven, 2007.

[3] T. H. Stix, "Decay of poloidal rotation in tokamak plasmas," *Physics of Fluids*, vol. 16, no. 3, pp. 1260–1267, 1973.

[4] R. J. LaHaye, "Islands in the stream: The effect of plasma flow on tearing stability," *Phys. Plasmas*, vol. 17, no. 056110, 2010.

[5] A. M. Garofalo *et al.*, "Sustained stabilization of the resistive-wall mode by plasma rotation in the DIII-D tokamak," *Phys. Rev. Lett.*, vol. 89, no. 23, 2002.

[6] H. Reimerdes *et al.*, "Effect of resonant and non-resonant magnetic braking on error field tolerance in high beta plasmas," *Nuclear Fusion*, vol. 49, no. 115001, 2009.

[7] F. L. Hinton and M. R. Rosenbluth, "The mechanism for toroidal momentum input to tokamak plasmas from neutral beams," *Physics Letters A*, vol. 259, pp. 267–275, June 1999.

[8] J. L. Luxon, "A design retrospective of the DIII-D tokamak," *Nuclear Fusion*, vol. 42, pp. 614–633, 2002.

[9] K. C. Shiang *et al.*, "Neoclassical transport fluxes in the plateau regime in nonaxisymmetric toroidal plasmas ," *Physics of Fluids*, vol. 29, no. 521, 1986.

[10] A. M. Garofalo *et al.*, "Plasma rotation driven by static nonresonant magnetic fields," *Phys. Plasmas*, vol. 16, p. 056119, 2009.

[11] J. Scoville, "Simultaneous feedback control of plasma rotation and stored energy on the DIII-D tokamak," in *Proceedings of the 24th Symposium on Fusion Technology, Warsaw, Poland*, 2006.

[12] J. Wesson, *Tokamaks*. Oxford, UK: Clarendon Press, 1984.

[13] R. J. Goldston, "Basic physical processes of toroidal fusion plasmas," *Proc. Course and Workshop Varenna, 1985*, vol. 1, pp. 165–186, 1986.

[14] P. A. Politzer and G. D. Porter, "Power threshold for neutral beam current drive," *Nuclear Fusion*, vol. 30, no. 1605, 1990.

[15] J. Barton *et al.*, "Physics-based control-oriented modeling of the safety factor profile dynamics in high performance tokamak plasmas," in *Proceedings of the 52nd IEEE Conference on Decision and Control, Florence, Italy*, 2013.

[16] J. D. Callen, A. J. Cole, and C. C. Hegna, "Toroidal rotation in tokamak plasmas," *Nucl. Fusion*, vol. 49, no. 8, p. 085021, 2009.

[17] W. Solomon *et al.*, "Advances in understanding the generation and evolution of the toroidal rotation profile on DIII-D," *Nucl. Fusion*, vol. 49, p. 085005, 2009.

[18] ITER Physics Basis, *Nuclear Fusion*, vol. 39, p. 2137, 1999.

[19] Y. Ou, C. Xu, and E. Schuster, "Robust control design for the poloidal magnetic flux profile evolution in the presence of model uncertainties," *IEEE Transactions on Plasma Science*, vol. 38, pp. 375–382, 2010.

[20] A. Packard, "What's new with μ: Structured uncertainty in multivariable control," Ph.D. dissertation, UC Berkeley, 1988.

[21] J. Barton, M. Boyer, W. Shi, E. Schuster *et al.*, "Toroidal current profile control during low confinement mode plasma discharges in DIII-D via first-principles-driven model-based robust control synthesis," *Nuclear Fusion*, vol. 52, no. 123018, 2012.

[22] S. Skogested and I. Postlethwaite, *Multivariable Feedback Control*. New York: John Wiley and Sons, Ltd, 2003.